JOURNAL OF MATERIALS SCIENCE 22 (1987) 1815–1826

High temperature deformation of titanium diboride

JEFFREY R. RAMBERG, WENDELL S. WILLIAMS
Department of Ceramic Engineering and Materials Research Laboratory, University of Illinois at Urbana-Champaign, Urbana, Illinois 61801, USA

Specimens of high purity polycrystalline titanium diboride, TiB_2, were tested in uniaxial compression under vacuum at a strain rate of $5 \times 10^{-4} sec^{-1}$ to determine the plastic yield behaviour. Generally, plastic deformation was detected only above 1700° C. The apparatus was able to apply a stress of 900 MPa at a maximum temperature of 2000° C. The yield stress data fit an Arrhenius function, with an apparent activation energy of $0.8 eV atom^{-1}$. Dislocation glide over the Peierls barrier is thought to be the deformation mechanism. The dependence of the yield stress on the grain size obeyed the Hall–Petch relation within the bounds of experimental error. A TiB_2 single crystal containing TiC precipitates was also compression-tested at 2000° C, and its yield stress was approximately four times the stress predicted by the Hall–Petch expression for a pure TiB_2 single crystal, suggesting that the precipitate raises the yield stress but that the intrinsic lattice resistance is still significant. Submicrometre-sized graphite inclusions were observed in the polycrystalline specimens, but are thought not to have a direct effect on the yield stress in the temperature regime of the present study.

1. Introduction

Although most research on structural ceramics has focused on fracture toughness, failure at extremely high temperatures may be a consequence of plastic deformation rather than brittle fracture. Hence studies of both kinds of mechanical response are in order.

We present the results of a study of the plastic deformation of titanium diboride, TiB_2, a material which holds some promise as a structural ceramic. The K_{Ic} value of single-phase TiB_2, for example, [1] surpasses that of transformation-toughened ZrO_2 above 1100 K, and we find that the high temperature plastic yield stress of TiB_2 is exceptionally high.

In an earlier study on the isomorphic compound ZrB_2, Haggerty and Lee [2] observed a ductile–brittle transition temperature around 2125° C, and they attributed the material's resistance to plastic flow to the presence of lamellar, or plate-shaped precipitates lying on the basal and prismatic planes of the hexagonal ZrB_2 crystal. Lamellar precipitates have also been observed on prismatic planes of TiB_2 [3, 4]. Williams and Ruggiero [3], using X-ray diffraction (XRD), showed that these precipitates have cubic symmetry, and Mochel *et al.* [5] later identified the precipitates as TiC by electron diffraction (ED) and electron energy loss spectroscopy (EELS).

Precipitates can, of course, have a pronounced effect on mechanical behaviour. Williams noted that doping a TiC crystal with a few tenths of a per cent of boron dramatically inhibited softening at high temperatures [6]. Metallographic analysis revealed the presence of lamellar precipitates on the $\{1\,1\,1\}$ planes of the TiC matrix. Thermochemical and crystallographic considerations argued for the precipitates being TiB_2, a hypothesis confirmed by Venables [7] using electron diffraction and autoradiography. This earlier example of lamellar TiB_2 precipitates in a TiC matrix is thus the converse of the case of lamellar TiC precipitates in a TiB_2 matrix considered in the present study.

We have reported on the resistance to plastic flow offered by a polycrystalline TiB_2 specimen when subjected to an applied stress of 500 MPa at a temperature of some 1900° C [8]. Lamellar precipitates were absent; we therefore attributed the lack of plastic distortion to intrinsic lattice resistance — the Peierls stress. Further refinements in our apparatus have allowed us to achieve the temperatures and stress necessary to deform this material, and to study the influence of grain boundaries and graphite inclusions in polycrystalline specimens and of TiC precipitates in single-crystal specimens. This more extensive study is reported here.

2. Material characterization

With the exception of some single-crystal specimens provided by the Linde Division of the Union Carbide Company, the TiB_2 used in our compression tests arrived courtesy of H. Robert Baumgartner of the Barberton Technical Center of PPG Industries, Inc., Ohio. Unlike most other TiB_2 in existence, these samples are practically free of the lamellar TiC precipitates, in spite of the addition of carbon during the plasma synthesis process [9] for the purpose of controlling grain growth during pressureless sintering at temperatures near 2000° C. The precise temperature and time at temperature were modified to produce bodies having mean grain sizes of 2.4, 6.7, 12 and 23

0022–2461/87 $03.00 + .12

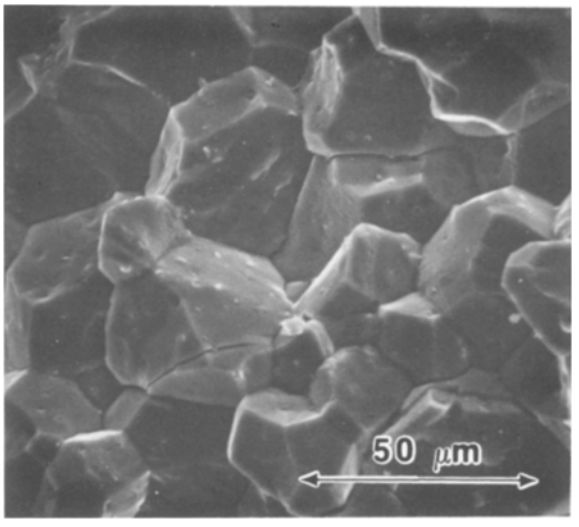

Figure 1 TiB_2 fracture surface showing equiaxed grains and sub-micrometre-sized inclusions.

micrometres as determined by the linear intercept method. All densities were greater than 99% of theoretical. PPG's elemental analysis of the material is as follows (wt %): Ti; 68.6, B; 30.6, C; 0.84, O; 0.03, N; 0.0005, all other metals each < 0.01.

Titanium and boron were analysed by quantitative chemistry, the other metals by emission spectroscopy, and carbon, oxygen and nitrogen by vacuum fusion.

The theoretical value for the weight ratio of titanium to boron in TiB_2 is 2.215; this analysis gives a ratio of 2.224, which would yield an empirical formula of $TiB_{1.97}$. The Ti–B phase diagram [10] (as in Fig. 5a) shows a rather narrow composition range for TiB_2, although some evidence exists for TiB_2 of greater boron deficiency [11–13].

The major impurity is carbon, but instead of manifesting itself as lamellar TiC precipitates, it occurs as elemental carbon and resides within TiB_2 grains as well as at the grain boundaries. The micrograph in Fig. 1 shows equiaxed TiB_2 grains and sub-micrometre nodules of impurity material. The EELS spectra in Fig. 2 indicate that the particles are pure carbon, and employing the ED pattern in Fig. 3b proves the carbon to be in the form of graphite.

By comparison, the chemical analysis of the TiB_2 crystal grown by the arc-Verneuil technique showed a much lower carbon concentration, 0.063 wt %, and

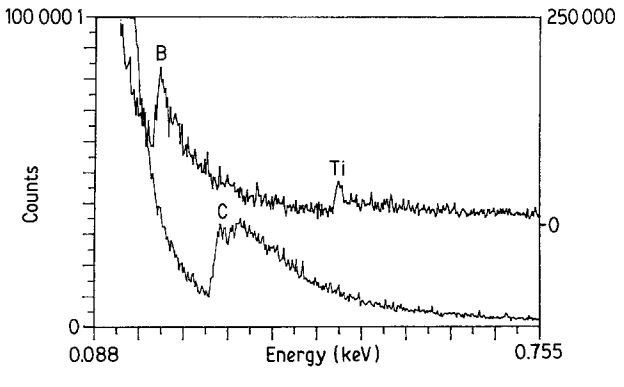

Figure 2 EELS spectra showing presence of titanium and boron in matrix (top spectrum), and carbon in impurity nodule (bottom spectrum).

oxygen and nitrogen levels of only a few parts per million. The micrograph of an etched crystal in Fig. 4 reveals an edge-on view of lamellar TiC precipitates. A carbon impurity in TiB_2 may thus occur as graphite or as TiC. Moreover the Ti–B–C phase diagram in Fig. 5b shows that TiB_2, TiC, and C can all co-exist at equilibrium [10].

3. Experimental procedure

Right rectangular prisms 1 by 1 by 2 mm were cut from larger TiB_2 bars using electric-discharge machining. Each face was ground to a 30 μm surface finish (Minimet Grinder/Polisher, Buehler Ltd, Lake Bluff, Illinois). A 5 min ultrasonic cleansing in methanol followed. Once in the test rig (see Fig. 6), the specimens were taken to the desired test temperature under vacuum. An optical pyrometer (Model No. 95, The Pyrometer Instrument Co., Northvale, New Jersey) monitored the specimen temperature with a precision of $\pm 10°$ C and an accuracy of $\pm 25°$ C. Uniaxial compression was supplied by a testing machine (Instron Corporation, Canton, Massachusetts) whose crosshead moved at the constant velocity of 1.67×10^{-6} m sec^{-1} (0.01 cm min^{-1}). A 100 kg load cell allowed the force to be monitored on a chart recorder (Model 194, Honeywell, Inc., Ft. Washington, Pennsylvania). The uncertainty in the applied stress was estimated to be $\pm 10\%$. Macroscopic plastic yielding was indicated as a deviation from linearity of stress against strain, or force against time as displayed on the chart recorder.

For the four grades of polycrystalline TiB_2 tested, the yield stress was evaluated both as a function of grain size and of temperature. The TiB_2 single crystal containing lamellar TiC precipitates was also compression tested. The crystal was cut such that the stress axis was perpendicular to the crystallographic c axis to provide a favourable orientation for prismatic slip. The Schmid factor for the $\{1\,0\,\bar{1}\,0\}\langle 1\,1\,\bar{2}\,0\rangle$ slip system was then calculated to be between 0.43 and 0.5.

4. Results

In the temperature regime 1700 to 2000° C, the yield stress of polycrystalline TiB_2 was found to decrease from 100 kg mm^{-2} (980 MPa) to 28 kg mm^{-2} (270 MPa). Fig. 7 shows yield stress plotted as a function of temperature for the various mean grain sizes of TiB_2 tested. The TiB_2 of 23 μm mean grain size proved to be more deformation-resistant below 1750° C than the samples of grains averaging 12 μm.

The decrease in yield stress with increasing temperature was exponential, with an apparent activation energy ranging between 0.7 and 1.3 eV atom^{-1} as calculated by taking the slope of log yield stress versus $1/T$. This Arrhenius form of the yield stress data is shown in Fig. 8.

At constant temperature, the yield stress decreased with increasing grain size except where noted above. The data were analysed using the Hall–Petch equation, and by extrapolation, a theoretical estimate was made of the shear strength of a precipitate-free TiB_2 single crystal at 2000° C. The experimentally obtained critical resolved shear stress on the prismatic slip system of a TiB_2 single crystal containing precipitates of TiC was

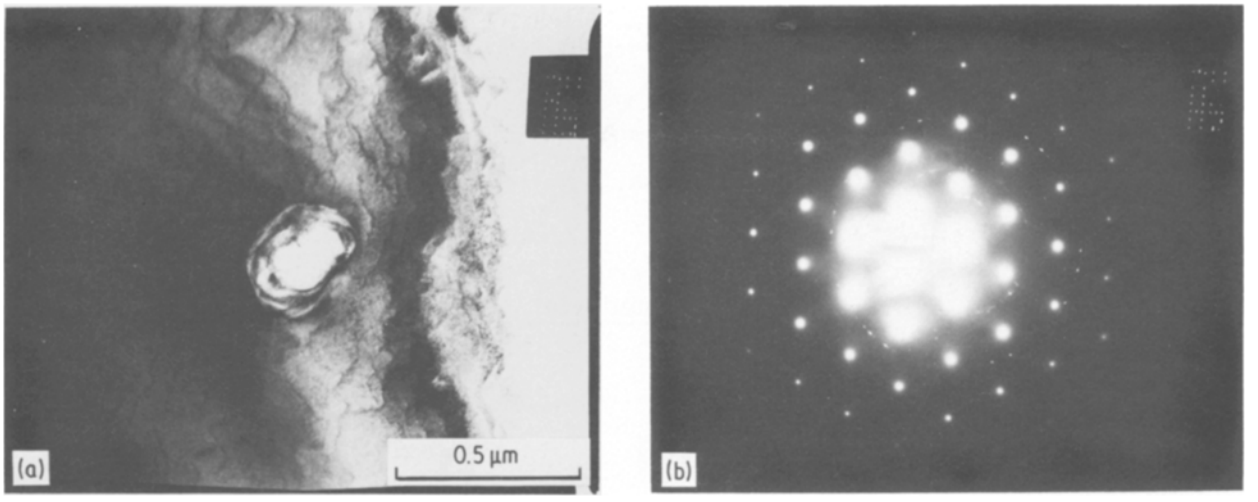

Figure 3 (a) Bright field image of matrix and inclusion, and (b) selected area diffraction image of same. The hexagonal pattern is from the TiB_2 matrix. The faint rings derive from the inclusion and were indexed to graphite.

approximately a factor of four greater than this estimated value. Fig. 9 shows the Hall–Petch form of the data.

5. Discussion

5.1. Yield strength comparison

Fig. 10 gives an overview of the yield stress against temperature profile for titanium diboride and compares its resistance to plastic yielding to that of other structural ceramics. It is interesting to note that at 1600° C, aluminium oxide has all but lost its structural integrity, while titanium diboride maintains a strength in the neighbourhood of a gigapascal. To the authors' knowledge, only silicon carbide prepared by chemical vapour deposition possesses a greater yield strength. [Authors' note: NC-430 is a silicon-rich reaction-bonded silicon carbide. Its yield stress data presented in Fig. 10 was extrapolated from creep data taken at much lower strain rates, and probably represents a lower bound.]

5.2. Deformation mode

The yield stress data fit an Arrhenius function fairly well (correlation coefficients around 0.95), suggesting that macroscopic deformation of polycrystalline TiB_2 at high temperatures at plastic strain rates on the order of 5×10^{-4} sec^{-1} is thermally activated.

Different methods of calculating activation energies of plastic deformation have been used by different workers. Investigators using constant-crosshead-speed testing machines to study plastic flow often report their results by the following convention:

$$\tau = \tau_0 \exp(E/kT) \quad (1)$$

where τ is the shear stress for plastic flow, τ_0 is a fitting parameter, E is the activation energy of plastic flow, and k and T have their usual significance.

Those investigators doing creep studies usually report their data in the form:

$$e_p = B\varrho \boldsymbol{b}(\tau/\tau_0)^n \exp(-Q/kT) \quad (2)$$

Here e_p is the plastic strain rate; B is a proportionality constant; ϱ and $\boldsymbol{b}$ represent the dislocation density and the magnitude of the Burgers vector, respectively; n is the stress exponent, and Q is the activation energy of plastic straining.

Solving Equation 2 in terms of τ and comparing to Equation 1 suggests that E and Q are not equal, although there is no *a priori* reason to believe that both equations cannot describe the same deformation process. Indeed, Haasen [14] identifies the yield region with stationary creep – a region of the sigmoidal creep strain against time curve where the rate is briefly constant and high, before steady-state creep is established at a lower rate.

We choose to express our data in terms of Equation 2 for several reasons:

1. Equation 2 contains more information than does equation 1;
2. Equation 2 facilitates comparisons with creep studies;
3. Equation 2 is based on a physical model of mobile dislocations, whereas Equation 1 is not based on any physical model. We therefore refer to E as the apparent activation energy and to Q as the true activation energy of plastic yielding.

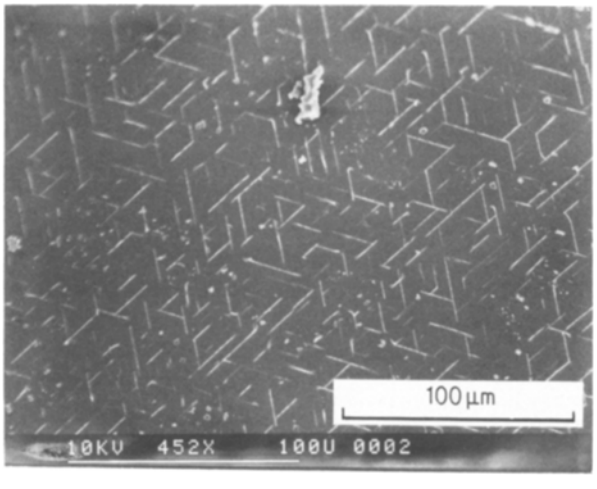

Figure 4 SEM micrograph of basal plane of TiB_2 crystal giving edge-on view of lamellar, prismatic plane precipitates.

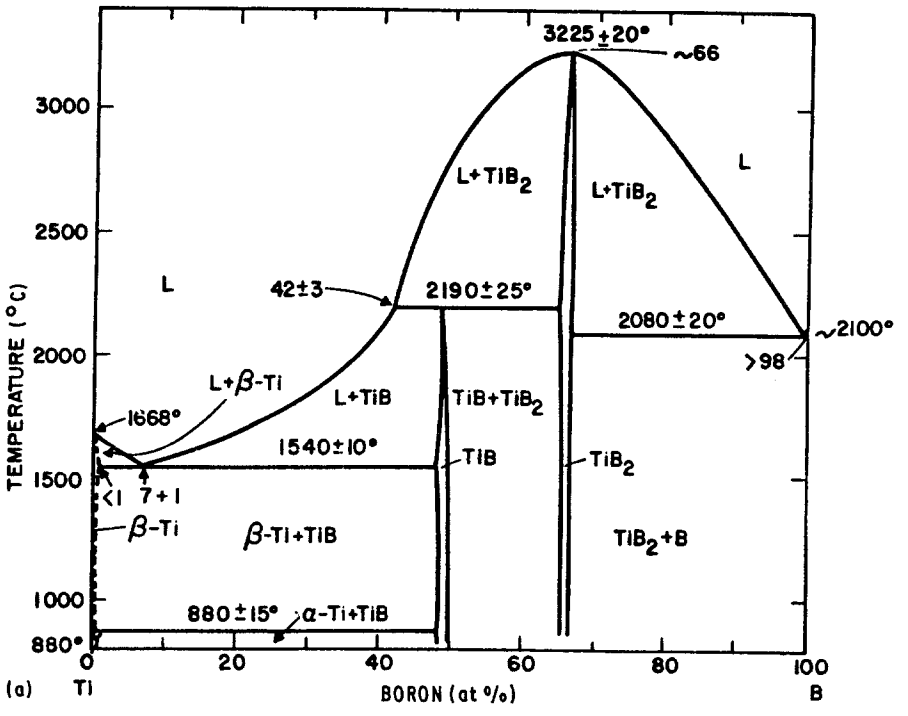

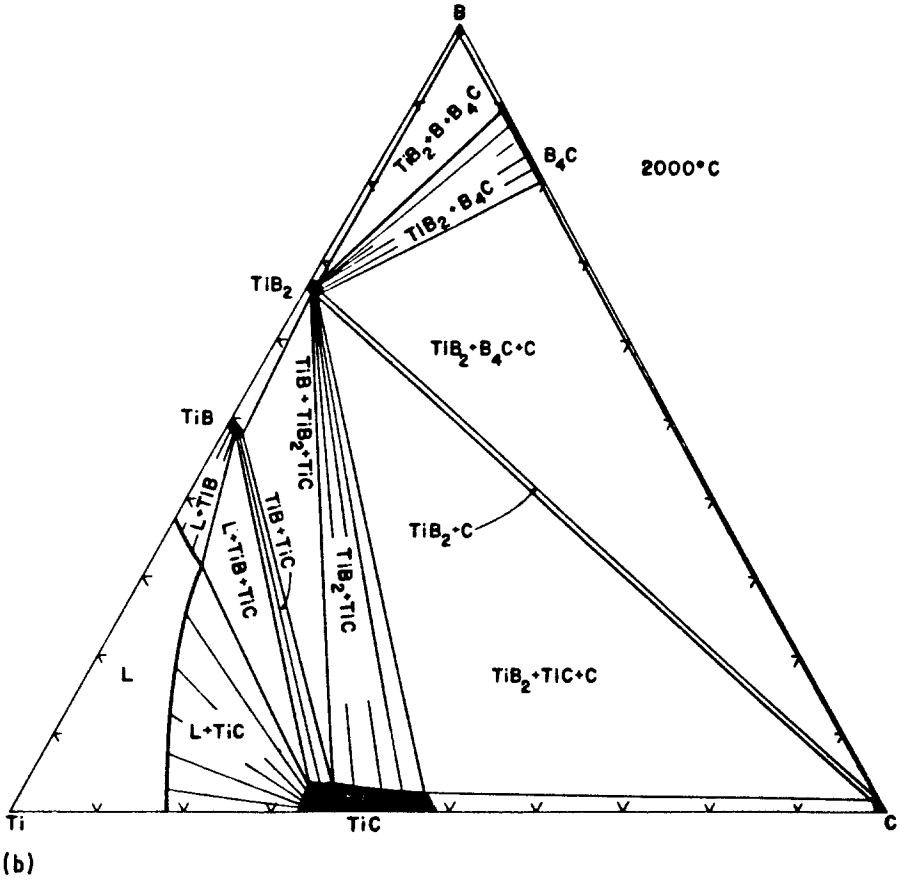

(b)

Figure 5 (a) The Ti–B binary phase diagram and (b) an isothermal section from the Ti–B–C ternary phase diagram. After Rudy [13].

The plastic strain rate model of Equation 2 is developed as follows:

$$e_p = \varrho b v \tag{3}$$

where v is the velocity of a single screw dislocation.

The velocity can be empirically related to the applied stress by the following equation:

$$v = (\tau/\tau_0)^n \tag{4}$$

where τ is the applied shear stress, τ_0 is that shear stress producing unit velocity, and n is the stress exponent.

The temperature-dependence of the dislocation velocity is assumed to obey a Boltzmann relation; thus

$$v = B(\tau/\tau_0)^n \exp(-Q/kT) \tag{5}$$

Substituting Equation 5 into Equation 3 results in the classic creep expression of Equation 2.

From creep studies on hot-pressed TiB_2, Mandorf *et al.* [15] report a stress exponent of 2. Despite some rather high impurity levels and porosity levels of 3 to 7%, this number appears to be in the correct range for a strongly bonded substance such as TiB_2. By way of comparison, n is in the range 1 to 2 for the covalent elements silicon and germanium [16], between 1 and

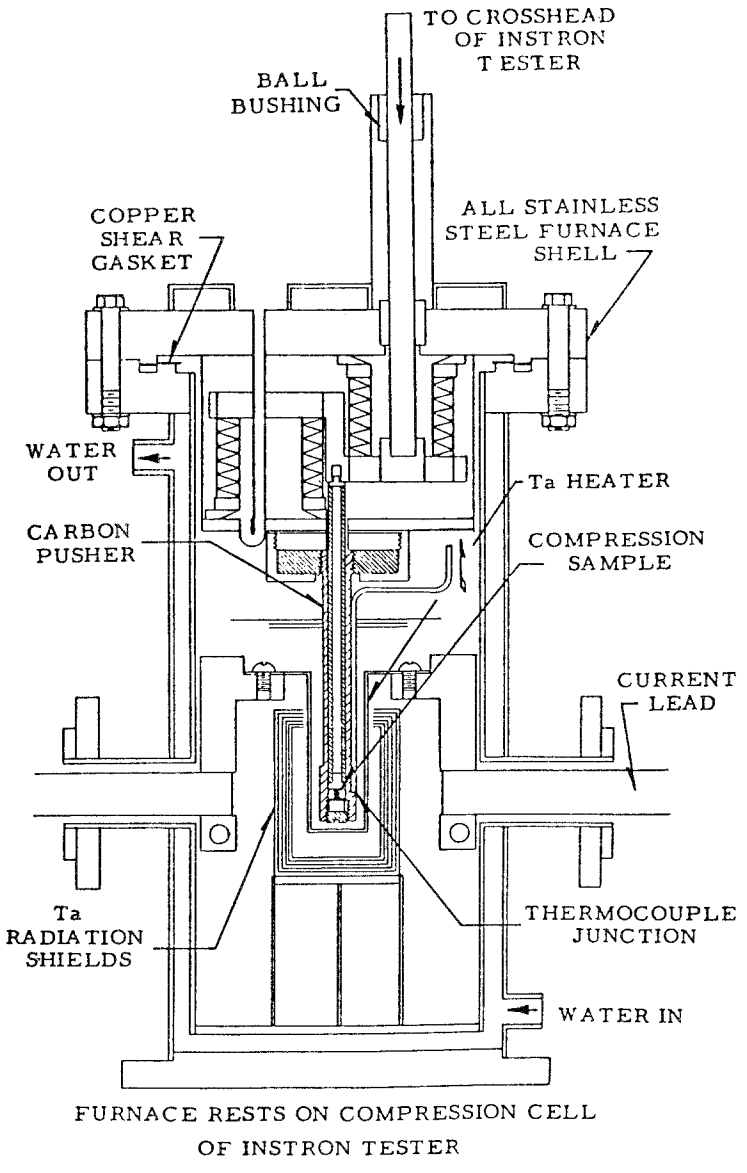

Figure 6 Cross-section of furnace and compression rig.

10 for TiC [17], but can be 100 or greater for the fcc metals.

From our compression measurements, the apparent activation energy for plastic flow in TiB_2 is 0.8 eV atom^{-1}, so the actual activation energy for plastic flow is then $0.8 \times 2 = 1.6$ eV atom^{-1}. The activation energies of other strong solids deforming by lattice-controlled dislocation glide are close to this value: 2.3 to 3.3 eV atom^{-1} for TiC [18, 19], 1.5 to 1.9 eV atom^{-1} for NbC [19], and 1.4 to 1.5 eV atom^{-1} for silicon and germanium [20].

Frost and Ashby [21] express these activation energies in terms of a parameter Gb^3, where G is the shear modulus and b is the length of the shortest Burgers vector. The resistance to dislocation motion is then characterized as strong, medium, or weak, depending on the nature of the impediment. The intrinsic lattice resistance is considered a weak obstacle, whose activation energy is $< 0.2Gb^3$. Strong obstacles, such as dispersions and strong precipitates, require activation energies of some $2Gb^3$ for a pinned dislocation to break free. Expressed in this manner, the activation energy for plastic flow in TiB_2 under the conditions of

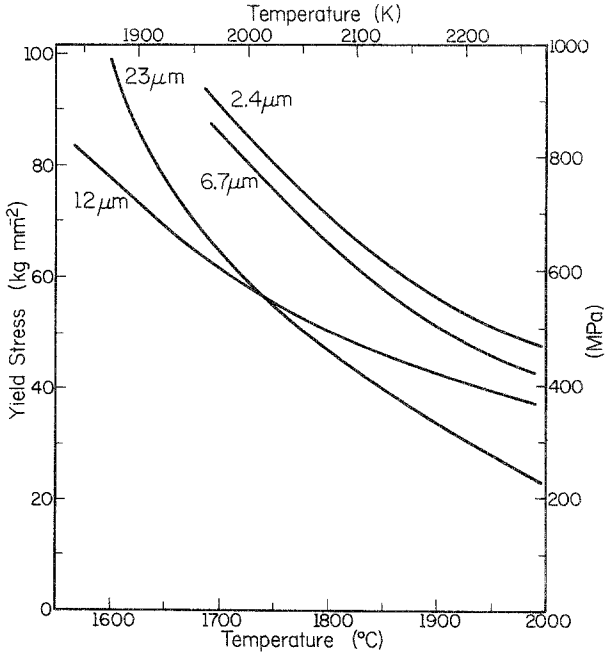

Figure 7 Stress producing general yielding against temperature for the four grades of polycrystalline TiB_2 tested. The TiB_2 of 23 μm grain size may contain TiC precipitates.

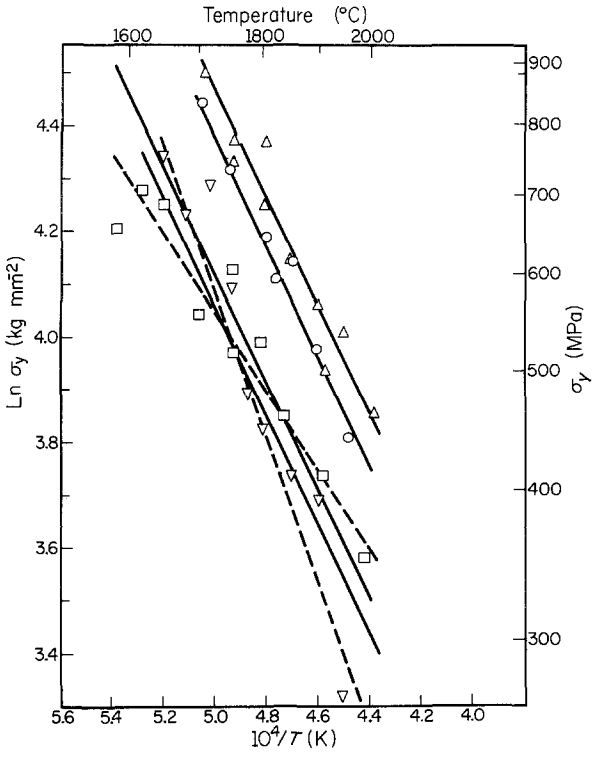

Figure 8 Log field stress against $1/T$ for the four grades of TiB_2 tested. The apparent activation energy ranges from 0.7 eV atom^{-1} for the 12 μm-sized grains to 1.3 eV atom^{-1} for the 23 μm polycrystals. Mean grain size (△) 24 μm, (○) 6.7 μm, (□) 12 μm, (▽) 23 μm.

our tests is $0.058Gb^3$. The force resisting plastic flow is therefore a weak one (comparatively), for which the Peierls force would qualify. Similarly, the corresponding activation energies for the other strong solids are 0.10 to $0.14Gb^3$ for TiC, 0.053 to 0.067 for NbC, and 0.20 for silicon and germanium.

If dislocation glide is indeed the mode of plastic yielding in TiB_2, then Equation 2 must be modified, because the dislocation density, ϱ, is not constant; it increases in direct proportion to the plastic strain. The yield stress increases as the square root of the plastic strain; thus, ϱ increases as the square of the stress required to continue plastic flow. One writes

$$\varrho = C\tau^2 \text{ or } \varrho = C'(\tau/\tau_0)^2 \quad (6)$$

and this produces the modified creep equation

$$e_p = B'\boldsymbol{b}(\tau/\tau_0)^{n+2} \exp(-Q/kT). \quad (2a)$$

Solving this equation in terms of τ and comparing to Equation 1, one can identify the constant τ_0' of Equation 1 with the constant term $\tau_0(e_p/B'\boldsymbol{b})^{1/(n+2)}$ of Equation 2a. Equating the Boltzmann factors shows that

$$Q = (n + 2)E \quad (7)$$

In other words, the apparent activation energy calculated by taking the slope of ln σ_y against $1/T$ must be multiplied by the factor $n + 2$ to reveal the true activation energy of plastic yielding, and to properly compare deformation data from incremental loading tests to that from dead load; i.e., creep tests. From Equation 7, the true activation energy of plastic distortion in TiB_2 under our particular test conditions is not 0.8 or 1.6 eV atom^{-1}, but 4 × 0.8 or 3.2 eV atom^{-1}. Compared to the activation energies of dislocation glide in the transition metal carbides and in silicon and germanium, 3.2 eV atom^{-1} may seem anomalously high. Nevertheless, an activation energy of 3.2 eV atom^{-1} translates to $0.12Gb^3$ for TiB_2 and still falls into the category of "weakly pinned dislocation" by the criterion of Frost and Ashby.

At temperatures above about half of the absolute melting temperature, as employed here, (T_m = 3225° C) the deformation mechanism is often dislocation climb, which is a diffusion-controlled process. Although the activation energies for self-diffusion in TiB_2 are not available, the activation energy for the diffusion of carbon in TiC is 4 to 5 eV atom^{-1} [22]; the diffusion of boron in TiB_2 is expected to require even

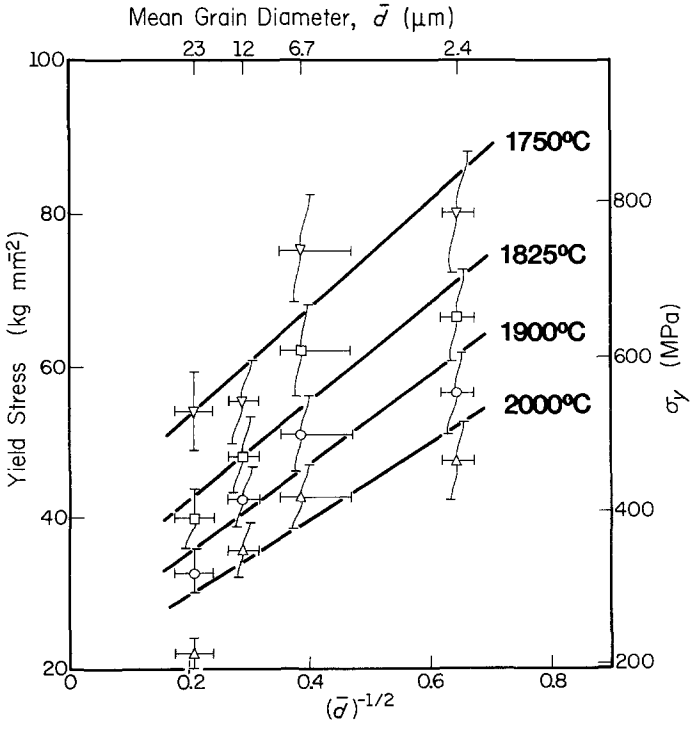

Figure 9 Yield stress against reciprocal square root of mean grain size (Hall–Petch plot).

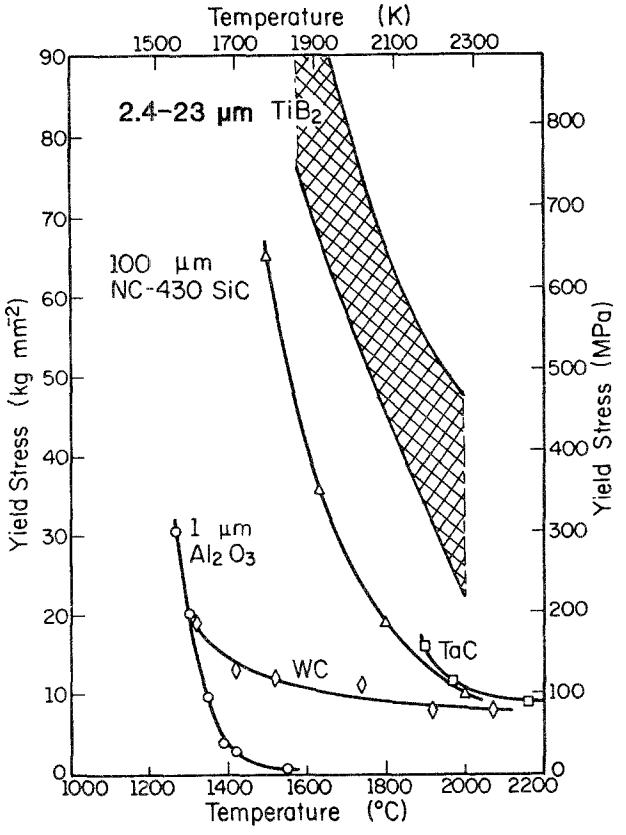

Figure 10 A summary of yield stress data for several structural ceramics. Data references: Al_2O_3, [35]; WC, [19]; TaC, [36]; SiC, [37].

more energy than that for carbon in TiC, as energy would be required to create vacancies. In TiC, many non-metal vacancies are already present. Further, the activation energy for the self-diffusion of titanium in TiC is 8 eV atom^{-1} [23]. Here the diffusion process would be rate-limited by the slowest diffusing species, which, for TiB_2, is likely to be the titanium atoms, as is the case for TiC. For this reason we believe that the deformation mechanism in polycrystalline TiB_2 under our test conditions is not dislocation climb but rather dislocation glide over the Peierls barrier.

5.3. Slip systems in TiB_2

The optical micrographs in Fig. 11 are of polished faces of TiB_2 specimens of each mean grain size studied after deformation at high temperature (1900 to 2000° C). All as-received specimens except the 2.4 μm grade TiB_2 showed some microcracking due to thermal expansion anisotropy with the extent of cracking increasing with increasing grain size. Failure by fracture was observed only in specimens containing the largest grains at temperatures below 1700° C and applied stresses of 100 kg mm^{-2}, although some other specimens of this material were plastically deformed as much as 16% at higher temperatures. To accommodate such a large deformation, there must either be five independent slip systems operating as required by von Mises [24], or some other deformation mechanism must be assisting a smaller number of slip systems. Such other mechanisms might include dislocation climb, grain-boundary sliding, or deformation twinning.

The other proposed mechanisms are not believed to be operating in these tests because:

1. twins have not been observed in deformed TiB_2 specimens;
2. the observed activation energy is too low for dislocation climb or Nabarro–Herring creep, as indicated above;
3. for Coble creep or grain-boundary sliding, the yield stress should decrease with increasing grain-boundary area; i.e., smaller mean grain size; yet the opposite is observed.

With other deformation mechanisms ruled out, we are left with dislocation glide. However, hexagonal crystals, especially the close-packed metals, cannot accomodate general yielding without the activation of pyramidal slip because prismatic and basal slip only provide four independent slip systems. The pyramidal slip system $\{10\bar{1}1\}\langle 11\bar{2}0\rangle$ is generally activated only at very high stresses because of the close spacing of the $\{10\bar{1}1\}$ planes.

On the other hand, the structure of TiB_2 is very different from that of the h c p metals. In the ideal h c p lattice the c/a ratio is 1.63; in TiB_2, which is simple hexagonal, it is 1.07. This reduced c/a ratio can easily be rationalized by imagining the substitution of boron for the B layer of titanium in the ABABAB packing sequence of elemental titanium.

In TiB_2, the most widely spaced planes are the basal planes, and the shortest lattice translation vectors are in the crystallographic a directions. One therefore expects $(0001)\langle 11\bar{2}0\rangle$ to be an active slip system. The second most widely spaced family of planes are the prismatic planes; therefore, $\{10\bar{1}0\}\langle 11\bar{2}0\rangle$ should also be an active slip system. In most hexagonal metals, be they close-packed or not, these are the most easily activated slip systems.

The basal and prismatic slip planes each contribute two independent slip systems. The additional slip system required for accommodating an arbitrary shape change should involve planes and directions of high atomic density. $\{10\bar{1}0\}[0001]$ is such a slip system, but it is not generally active in h c p structures because of the large lattice distortion necessary at the mid-slip configuration. TiB_2 is not a close-packed structure, and the lattice need only dilate a little more for $\{10\bar{1}0\}[0001]$ slip than for $\{10\bar{1}0\}\langle 11\bar{2}0\rangle$ slip (0.080 against 0.060 nm). Such a slip mechanism yields two more independent slip systems and the grain can deform arbitrarily without resorting to the very difficult pyramidal slip system. Of the dislocations observed in thin foils of ZrB_2 by Haggerty and Lee [2], none had Burgers vectors in the direction of the crystallographic c-axis, although those authors saw no reason why dislocations of such orientation might be precluded.

Nakano *et al.* [25] performed microhardness measurements on TiB_2 single crystals between room temperature and 1000° C. Not only were they able to obtain dislocation glide on the $\{10\bar{1}0\}[0001]$ slip system, their data suggest that this system is the primary slip system above approximately 500° C. Moreover, they were able to activate dislocation glide on two other slip systems, the $(0001)\langle 10\bar{1}0\rangle$ and the

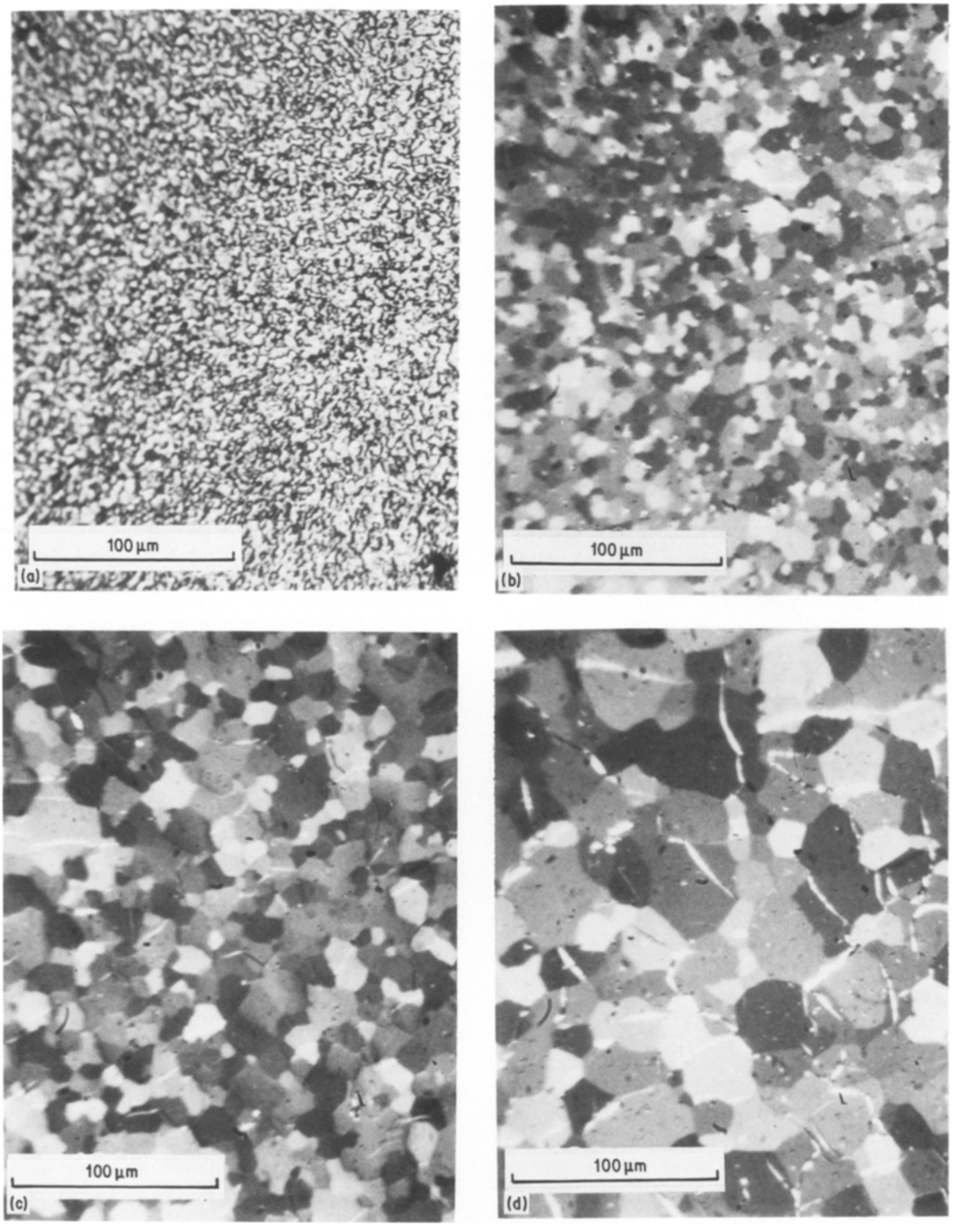

Figure 11 Optical micrographs of the four grades of polycrystalline TiB_2 after plastic deformation at high temperatures. The cracks are not the result of compression-testing, but of thermal expansion anisotropy after sintering. Average grain sizes (μm): (a) 2.4, (b) 6.7, (c) 12, (d) 23.

$\{1\,1\,\bar{2}\,0\}\langle 1\,\bar{1}\,0\,0\rangle$. Thus we see that TiB_2 indeed has a sufficient number of slip systems to accommodate the constraints imposed by polycrystalline deformation. In addition, either dislocations with *c*-axis Burgers vectors exist, or partial dislocations exist whose total Burgers vector is in the [0 0 0 1] direction.

5.4. Influence of lamellar precipitates on the yield stress

The TiB_2 single crystal which was compression tested was oriented in the compression rig such that $\{1\,0\,\bar{1}\,0\}\langle 1\,1\,\bar{2}\,0\rangle$ slip was favoured. Plastic deformation should have occurred with only this slip system operating (the

Schmid factor was zero for the $(0\,0\,0\,1)\langle 1\,1\,\bar{2}\,0\rangle$ slip system). Deformation of this single crystal was difficult and was induced only after stressing to 52 kg mm^{-2} (510 MPa) at 2000° C. At this temperature the crystal thus showed a yield strength on a par with that of fine-grained TiB_2 ($d = 2.4\,\mu$m). We believe the explanation for this yield stress is the presence of lamellar TiC precipitates on the prismatic planes of the TiB_2 crystal.

In the 1971 study on the plastic deformation of ZrB_2 single crystals, Haggerty and Lee concluded that the oriented lamellar precipitates were controlling the deformation. They observed brittle behaviour at 1490 and 2000° C, fracturing test specimens at applied stresses of 15.8 and 8.9 kg mm^{-2}. Ductility was achieved at 2125° C with resolved shear stresses at the upper and lower yield points of 3.45 and 2.18 kg mm^{-2}, respectively. Earlier metallographic examination by Leombruno *et al.* [26] showed plate-like precipitates on basal planes and precipitates with a ribbon-like morphology on prismatic planes. Based on a calculation of the stress required to drive a dislocation past an obstacle and the size, shape and spacing of these obstacles (namely, the lamellar precipitates), Haggerty and Lee concluded that slip was occurring on basal planes and regulated by the prismatic precipitates.

By way of comparison, our TiB_2 crystal contained these Widmanstaetten precipitates on prismatic planes at roughly the same spacing as those in Haggerty and Lee's ZrB_2 crystal, some 4 to 5 μm apart. Unlike their ZrB_2, however, basal plane precipitates were not found in the TiB_2 specimens, although such precipitates have been observed previously [27]. Moreover, fracture did not occur during compression tests at 1720 and 1910° C, even though compressive stresses of some 70 kg mm^{-2} were applied.

The shear stress required to push a dislocation past an obstacle is given by [28]

$$\tau = Gb/d \qquad (8)$$

where τ is the shear stress required to free the dislocation, G is the shear modulus, $\boldsymbol{b}$ is the magnitude of the Burgers vector, and d is the distance between obstacles. Substituting values of 180 GPa for the shear modulus of TiB_2 at 2000° C, 0.3028 nm for $\boldsymbol{b}$ (length of crystallographic a axis), and 4 μm for d, one calculates a blocking stress of only 14 MPa or about 1.4 kg mm^{-2}, which is close to the value calculated by Haggerty and Lee for ZrB_2. This proposed mechanism, then, does not seem to be applicable to the present study, and it may have been coincidental that the calculated "unpinning" shear stress was so close to the critical resolved shear stress of the ZrB_2 crystal tested at 2125° C by Haggerty and Lee.

The lamellar precipitates in the TiB_2 crystal have been shown to be TiC by ED and EELS as discussed earlier in this paper. We propose an alternative deformation mechanism for this material, namely Suzuki hardening. In this model, plastic deformation is controlled by the diffusion of boron into and carbon out of the precipitate in a manner analogous to the model put forth by Hoffman and Williams [29] concerning the deformation of TaC. They suggest that the deformation rate of TaC is limited by the diffusion of carbon into and out of a stacking fault whose composition is believed to be the hemicarbide Ta_2C [30]. The activation energy is expected to be quite different for this process than for that of pushing dislocations past obstacles. A study of the temperature dependence of the yield stress for precipitate-laden TiB_2 crystals should shed some light on the actual deformation mechanism.

5.5. Graphite inclusions in polycrystalline TiB_2

As mentioned earlier in this paper, the polycrystalline TiB_2 samples tested contain graphite impurity particles. If these inclusions play a role in the deformation of TiB_2, it is not by the pinning of dislocations. Employing the aforementioned equation regarding the shear stress necessary to free a dislocation from a pinning site, a 2 μm spacing between graphite particles gives a "breakaway" shear stress of some 28 MPa, which is still at least a factor of three lower than the shear stress developed in the specimen of least yield strength. Obstacle pinning by these graphite nodules is not expected to be rate-limiting to dislocation glide until temperatures in the 2100 to 2200° C range are reached, judging from the results of Haggerty and Lee.

5.6. Single-crystal against polycrystalline yielding

It may be possible to predict the yield stress of single crystals by extrapolating yield stress data of polycrystalline specimens back to the ordinate of a Hall–Petch plot. Some investigators [31] criticize this practice because often those doing the extrapolating fail to take into account the differences in the yielding criteria between single crystals and polycrystals.

As far as the onset of yielding is concerned, the chief difference is in the number of slip systems operating in the two cases. For the single crystal, only one slip system is activated initially, although others may later become active as the plastic strain increases, depending on the type of crystal. For completely accommodated plastic flow by dislocation glide in a polycrystalline material, five independent slip systems must be operating.

In many materials of hexagonal symmetry, there simply are not sufficient active slip systems for general yielding, and the result is cavitation or fracture. None of the specimens in the present study fractured when stressed at temperatures above 1700° C, and none showed cavitation, even though many were plastically strained 10 to 20%. In the temperature regime of our compression tests, we feel that the von Mises criterion is being met, and from planar and linear atomic density considerations, we think that the fifth slip system, the one responsible for general yielding in polycrystalline TiB_2, is the $\{1\,0\,\bar{1}\,0\}\,[0\,0\,0\,1]$ slip system.

A measure of the polycrystalline yield stress in TiB_2 is then a measure of the stress necessary to activate the $\{1\,0\,\bar{1}\,0\}\,[0\,0\,0\,1]$ system, and an extrapolation of Hall–Petch yielding data might then predict the critical resolved shear stress (CRSS) of this system in a single

crystal, but not necessarily the CRSS of more easily activated systems, like $\{1\,0\,1\,0\}\langle 1\,1\,2\,0\rangle$ or $(0\,0\,0\,1)\langle 1\,1\,\bar{2}\,0\rangle$.

Another complication in comparing the yield stress of a single crystal to a polycrystalline body lies in taking into account the orientation(s) of the slip system under study. In the single crystal, the orientation can be described precisely and for a given axis of applied stress, a given slip system has some particular Schmid factor to describe the fraction of applied stress resolved on the slip plane in the slip direction as a shear stress. In a polycrystal with (assumed) random crystallite orientations, one must calculate an effective Schmid factor, one which averages the resolved shear stress over all possible orientations. This number has been derived for certain Bravais lattices, and is called the Taylor factor, after its discoveror [32].

In many respects, the Taylor factor can be likened to a reciprocal Schmid factor, in that it expresses the ratio of the applied tensile or compressive yield stress to the glide yield stress:

$$\sigma_0 = Mi_0 \tag{9}$$

where σ_0 is the uniaxial yield stress, i_0 is the critical stress required for plastic shearing, and M is the Taylor factor.

The primary slip system in fcc metals is $\{1\,1\,1\}\langle 1\,\bar{1}\,0\rangle$. There are 12 slip modes in this system, five of which are independent. A polycrystalline fcc metal can thus accommodate an arbitrary deformation in this system alone. Taylor was able to plot "topographically" on a stereographic projection the various M factors for $\{1\,1\,1\}\langle 1\,\bar{1}\,0\rangle$ slip in fcc crystals [32]. He then averaged these factors over all orientations and found $M = 3.06$. The effective Schmid factor would then be 0.322. This value may seem unusually high in light of 0.5 being the maximum attainable Schmid factor, but one must keep in mind the many slip modes in the $\{1\,1\,1\}\langle 1\,\bar{1}\,0\rangle$ slip system.

A calculation of the average Taylor factor is probably more difficult for crystals that must activate more than one class of slip system; perhaps this accounts for the apparent lack of data for other crystal systems.

If the deformation-controlling slip system in polycrystalline TiB_2 is in fact the $\{1\,0\,\bar{1}\,0\}[0\,0\,0\,1]$ system, an averaged Taylor factor would allow us to estimate the critical resolved shear strength of this slip system. It is not likely that such a number is going to be found in the literature, so it must either be calculated or estimated. Calculation is beyond the scope of the present study, so an estimate seems in order.

With 12 possible slip modes in the $\{1\,1\,1\}\langle 1\,\bar{1}\,0\rangle$ system, the effective Schmid factor is 0.322. There are three slip modes in the presumed $\{1\,0\,\bar{1}\,0\}[0\,0\,0\,1]$ slip system of TiB_2; consequently one expects a smaller effective Schmid factor. A reasonable estimate might be 0.2. This may seem to be a very rough approximation, and it is. The comparison between single-crystal and polycrystalline yielding developed here, though, is also a crude comparison, as evidenced by the features which must be taken into account. This comparison, then, is meant to be taken qualitatively.

From the Hall–Petch plot shown in Fig. 9, an applied uniaxial stress of $25\,kg\,mm^{-2}$ should initiate plastic flow on the aforementioned slip system in a precipitate-free TiB_2 single crystal at 2000° C. The critical resolved shear stress on this slip system would then be $5\,kg\,mm^{-2}$. The TiB_2 crystal which was compression-tested contained lamellar TiC precipitates and yielded at an applied stress of $52\,kg\,mm^{-2}$ at 2000° C. The critical resolved shear stress on the $\{1\,0\,\bar{1}\,0\}\langle 1\,1\,\bar{2}\,0\rangle$ slip system was at least $22\,kg\,mm^{-2}$, and possibly as large as $26\,kg\,mm^{-2}$, depending on the exact Schmid factor. No CRSS data is yet available for the slip system in question, $\{1\,0\,\bar{1}\,0\}[0\,0\,0\,1]$, but the theory discussed earlier suggests that it would be somewhat larger than for the "ordinary" prismatic slip system.

The significance of this section lies in these numbers. Again, the comparison is not meant to be strictly quantitative, but notice the difference between a critical resolved shear stress of 5 and $22\,kg\,mm^{-2}$. Care was taken to try to "equalize" as much as possible the yield data for each material, and the numbers are still apart by a factor of four. If the numbers had been reversed, we might not have known what to make of such a result, but it is the precipitate-laden crystal which is more resistant to plastic yielding than the polycrystal, and this in spite of its yielding on what we believe is the more easily activated slip system. The polycrystalline TiB_2 specimens lack the lamellar TiC precipitates; the arc-grown TiB_2 single crystals are loaded with them. We believe that these precipitates are responsible for the high yield stress observed, just as lamellar TiB_2 precipitates in TiC single crystals raise the yield stress at high temperatures.

5.7. Grain size dependence of yield strength

Finally a word must be said about the isothermal yield strength dependence on the grain size of the specimens. The equation of Hall and Petch [33, 34]

$$\sigma_y = \sigma_0 + kd^{-1/2} \tag{10}$$

illustrates in theory how the presence of grain boundaries act as barriers to glissile dislocations. Here σ_0 represents the single-crystal yield strength and k the dependence of same on the reciprocal square root of the mean grain size. The graph of σ_y against $d^{-1/2}$ is shown in Fig. 9 and one sees a systematic deviation from the linear theoretical relationship. Perhaps the slightly different activation energies observed for different grain sizes are responsible for this non-linearity. Fig. 12 shows the original Hall–Petch data and the "revised" data in which the various yield stresses are calculated on the basis of a best fit to the curves assuming a constant $0.8\,eV\,atom^{-1}$ apparent activation energy for each specimen. The revised Hall–Petch plot is much more linear than the original, though this strategy suppresses any real dependence of the activation energy on grain size.

The yield stress data for the TiB_2 specimens of $23\,\mu m$ mean grain size must be considered with these two thoughts in mind: First, extensive microcracking, both transgranular and intergranular, may have the effect of reducing the apparent grain size. Second, some electron micrographs reveal what appear to be

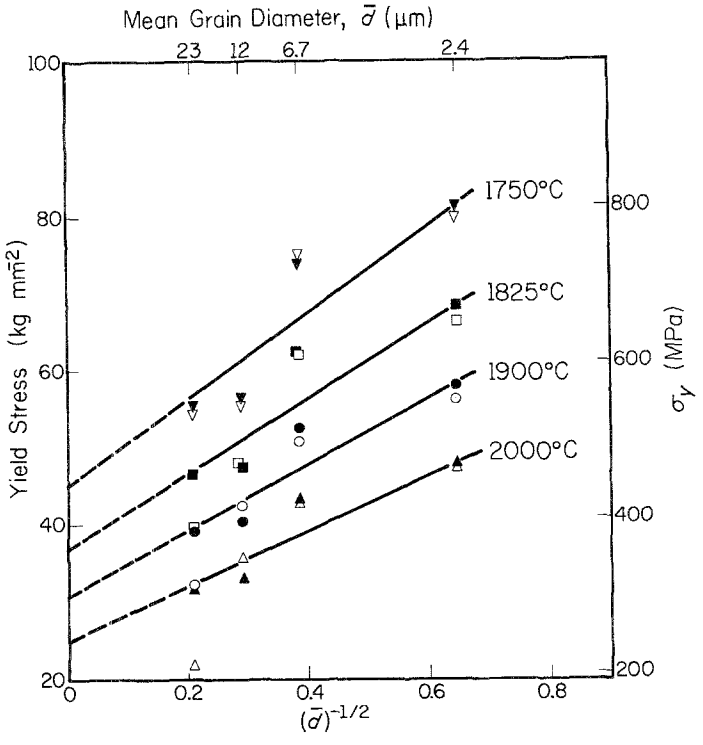

Figure 12 Original Hall–Petch form of the yield stress data (open polygons), and the revised Hall–Petch analysis (shaded polygons) based on best fit to lines of constant activation energy (0.8 eV atom^{-1}).

lamellar precipitates (see Fig. 13). It is not known to us if these are in fact such precipitates, and if they are, why similar precipitates were not observed in other specimens of the other grain sizes. All polycrystalline samples tested in our lab were processed from the same powder lot at PPG Industries, Inc. Both of these aberrations, though, might be expected to increase the specimen's yield strength.

Tempering the significance of the 23 μm yield stress data does not completely eliminate uncertainties due to experimental error, of course, as an inspection of the rest of the raw data will confirm. If, however, the variability in activation energy data for the other three grain size groups can be attributed to uncertainty in the experimental data, which is a reasonable explanation, then Fig. 12 illustrates the applicability of the Hall–Petch relation to the high temperature plastic deformation of TiB_2. The importance of dislocation/grain-boundary interactions implied will motivate further study of this system for a more detailed understanding of this exceptionally stable structural ceramic.

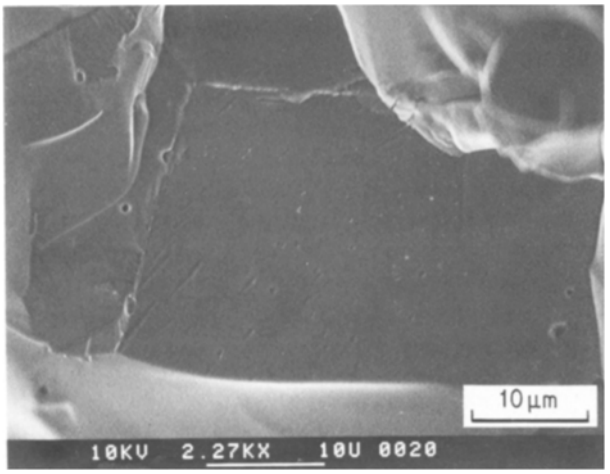

Figure 13 Possible precipitates in TiB_2 polycrystal. These 23 μm-sized grains were sintered at 2275° C, at which temperature precipitates in TiB_2 routinely coarsen.

6. Conclusions

1. With the exception of high purity SiC, the yield strength of TiB_2 is greater than any other ceramic compound for which such data exists.

2. High temperature plastic yielding of polycrystalline TiB_2 is a thermally activated process whose activation energy is 3.2 eV atom^{-1}.

3. In this study, the mechanism of plastic yielding of TiB_2 is dislocation glide.

4. At high temperatures and stresses, experimental results and theoretical models indicate that five or more independent slip systems can operate in TiB_2.

5. Grain boundaries influence the yield strength of polycrystalline TiB_2 via the Hall–Petch relation.

6. Graphite particles do not significantly influence the yield stress.

7. Lamellar TiC precipitates in TiB_2 increase the yield stress too much for dislocation pinning to be the mechanism responsible; a diffusion-controlled deformation process is being investigated.

Acknowledgements

The authors would like to thank Peggy Mochel for assistance with the electron diffraction work and Mark Hoffman for his help with acquiring the EELS data. We thank Clare Allocca for the fracture surface micrograph. The assistance of Nancy Finnigan regarding bulk chemical analysis is also acknowledged. This work was supported by the Materials Sciences Division of the Department of Energy under Contract No. DE-AC02-76ER0118 with the University of Illinois Materials Research Laboratory.

References

1. W. J. LACKEY, D. P. STINTON, G. A. CERNEY, L. L. FEHRENBACHER and A. C. SCHAFFHAUSER, "Ceramic Coatings for Heat Engine Materials – Status and

Future Needs", ORNL/TM-8959, Oak Ridge National Laboratory, Oak Ridge, Tennessee, USA (1985).
2. J. S. HAGGERTY and D. W. LEE, *J. Amer. Ceram. Soc.* **54** (1971) 572.
3. W. S. WILLIAMS and J. D. RUGGIERO, unpublished work (1960).
4. C. T. LYNCH, S. A. MERSOL and F. W. VAHLDIEK, *J. Less-Common Metals* **10** (1966) 206.
5. P. MOCHEL, C. ALLISON and W. S. WILLIAMS, *J. Amer. Ceram. Soc.* **64** (1981) 185.
6. W. S. WILLIAMS, *Trans. AIME* **236** (1966) 211.
7. J. D. VENABLES, *Phil. Mag.* **16** (1967) 873.
8. J. R. RAMBERG, C. F. WOLFE and W. S. WILLIAMS, *J. Amer. Ceram. Soc.* **68** (1985) C-78.
9. H. R. BAUMGARTNER and R. A. STEIGER, *J. Amer. Ceram. Soc.* **67** (1984) 207.
10. E. RUDY, "Ternary Phase Equilibria in Transition Metal-Boron-Carbon-Silicon Systems, Part V. Compendium of Phase Diagram Data, Air Force Materials Laboratory, Metals and Ceramics Division". (Wright-Patterson Air Force Base, Ohio, USA, 1969) p. 606.
11. R. FEURER, G. CONSTANT and C. BERNARD, *J. Less-Common Metals* **67** (1979) 107.
12. M. I. AIVAZOV and I. A. DOMASHNEV. *Izv. Akad. Nauk SSSR, Neorg. Mater.* **7** (1971) 1139.
13. K. NAKANO, H. HAYASHI and T. IMURA, *J. Crystal Growth* **24** (1974) 673.
14. P. HAASEN, "Plastic Flow and Strength of Germanium", in Proceedings of the Conference on the Relation between Structure and Strength in Metals and Alloys, Vol. 2, National Physical Laboratory, Teddington, Middlesex, UK, January 7–9, 1963 (Her Majesty's Stationery Office, London, 1963) p. 588.
15. V. MANDORF, J. HARTWIG and E. J. SELDIN, in "High Temperature Materials", Vol. 2, edited by G. M. Ault (Wiley-Interscience, New York, 1963) p. 455.
16. A. R. CHAUDHURI, J. R. PATEL and L. G. RUBIN, *J. Appl. Phys.* **33** (1962) 2736.
17. W. S. WILLIAMS, *J. Appl. Phys.* **35** (1964) 1329.
18. W. S. WILLIAMS, "Brittle-Ductile Behavior of the Transition Metal Carbides" in "Thermodynamic, Physical, and Structural Properties of Semimetallic Compounds (Proprietes Thermodynamiques, Physiques et Structurales des Derives Semimetalliques)". (Editions of the National Center for Scientific Research, Paris, 1967) p. 181.
19. A. KELLY and D. J. ROWCLIFFE, *J. Amer. Ceram. Soc.* **50** (1967) 253.
20. V. I. TREFILOV and YU V. MIL'MAN, *Soviet Physics Doklady* **8** (1964) 1240.
21. H. J. FROST and M. F. ASHBY, "Deformation-Mechanism Maps" (Pergamon Press, New York, 1982) p. 8.
22. S. SARIAN, "Diffusion of ^{44}Ti in TiC_x", *J. Appl. Phys.* **40** (1969) 3515.
23. S. SARIAN, *J. Appl. Phys.* **39** (1968) 5036.
24. R. VON MISES, *Z. Angew. Math. Mech.* **8** (1928) 161.
25. K. NAKANO, H. MATSUBARA and T. IMURA, *Jpn J. Appl. Phys.* **13** (1974) 1005.
26. W. J. LEOMBRUNO, J. S. HAGGERTY and J. L. O'BRIEN, *Mater. Res. Bull.* **3** (1968) 361.
27. W. S. WILLIAMS, C. ALLISON and P. MOCHEL, "Crystal Chemistry and Electron Energy Loss Spectroscopy of Titanium Carbide Precipitates in TiB_2", in "Science of Hard Materials", edited by R. K. Viswanadham, D. J. Rowcliffe and J. Gurland. (Plenum, New York, 1983) p. 169.
28. E. OROWAN, "Classification and Nomenclature of Internal Stresses", in Symposium on Internal Stresses in Metals and Alloys, London, October 15–16, 1947 (The Institute of Metals, London, 1948) p. 47.
29. M. P. HOFFMAN and W. S. WILLIAMS, "A Simple Model for the Deformation Behavior of Tantalum Carbide", *J. Amer. Ceram. Soc.* **69** (1986) 612.
30. C. ALLISON, M. P. HOFFMAN and W. S. WILLIAMS, *J. Appl. Phys.* **53** (1982) 6757.
31. U. F. KOCKS, *Met. Trans.* **1** (1970) 1121.
32. G. I. TAYLOR, *J. Inst. Metals* **62** (1938) 307.
33. E. O. HALL, *Proc. Phys. Soc. London.* **B64** (1951) 747.
34. N. J. PETCH, *J. Iron and Steel Inst.* **174** (1953) 25.
35. R. M. CANNON, W. H. RHODES and A. H. HEUER, *J. Amer. Ceram. Soc.* **63** (1980) 46.
36. H. A. JOHANSEN and J. G. CLEARY, *J. Electrochem. Soc.* **113** (1966) 375.
37. C. H. CARTER Jr and R. F. DAVIS, *J. Amer. Ceram. Soc.* **67** (1984) 409.

Received 8 July
and accepted 9 September 1986